Climate Dynamics (2025) 63:465
https://doi.org/10.1007/s00382-025-07880-9

ORIGINAL ARTICLE

Discontinuous stochastic forcing in Greenland ice core data

Keno Riechers[1] · Andreas Morr[2,3] · Klaus Lehnertz[4,5,6] · Pedro G. Lind[7,8] · Niklas Boers[2,3,9] · Dirk Witthaut[10,11] · Leonardo Rydin Gorjão[12,13]

Received: 22 February 2025 / Accepted: 15 September 2025 / Published online: 25 November 2025

Abstract

Paleoclimate proxy records from Greenland ice cores, archiving e.g. δ^{18}O as a proxy for surface temperature, show that sudden climatic shifts called Dansgaard–Oeschger events (DO) occurred repeatedly during the last glacial interval. They comprised substantial warming of the Arctic region from cold to milder conditions. Concomitant abrupt changes in the dust concentrations of the same ice cores suggest that sudden reorganisations of the hemispheric-scale atmospheric circulation have accompanied the warming events. Genuine bistability of the North Atlantic climate system is commonly hypothesised to explain the existence of stadial (cold) and interstadial (milder) periods in Greenland. However, the physical mechanisms that drove abrupt transitions from the stadial to the interstadial state, and more gradual yet still abrupt reverse transitions, remain debated. Here, we conduct a one-dimensional data-driven analysis of the Greenland temperature and atmospheric circulation proxies under the purview of stochastic processes. We take the Kramers–Moyal equation to estimate each proxy's drift and diffusion terms within a Markovian model framework. We then assess noise contributions beyond Gaussian white noise. The resulting stochastic differential equation (SDE) models feature a monostable drift for the Greenland temperature proxy and a bistable one for the atmospheric circulation proxy. Indicators of discontinuity in stochastic processes suggest to include higher-order terms of the Kramers–Moyal equation when modelling the Greenland temperature proxy's evolution. This constitutes a qualitative difference in the characteristics of the two time series, which should be further investigated from the standpoint of climate dynamics.

Keno Riechers, Andreas Morr and Leonardo Rydin Gorjão have contributed equally to this work.

✉ Andreas Morr
andreas.morr@tum.de

[1] Climate Physics, Max Planck Institute for Meteorology, Hamburg, Germany

[2] Earth System Modelling, School of Engineering and Design, Technical University of Munich, Munich, Germany

[3] Research Domain IV – Complexity Science, Potsdam Institute for Climate Impact Research, 14473 Potsdam, Germany

[4] Department of Epileptology, University of Bonn Medical Center, 53105 Bonn, Germany

[5] Helmholtz Institute for Radiation and Nuclear Physics, University of Bonn, 53115 Bonn, Germany

[6] Interdisciplinary Centre for Complex Systems, University of Bonn, 53175 Bonn, Germany

[7] Department of Computer Science, OsloMet – Oslo Metropolitan University, 0130 Oslo, Norway

[8] School of Economics, Innovation and Technology, Kristiania University of Applied Sciences, Kirkegata 24-26, 0153 Oslo, Norway

[9] Global Systems Institute and Department of Mathematics, University of Exeter, Exeter, UK

[10] Institute of Energy and Climate Research (IEK-10), Forschungszentrum Jülich, 52428 Jülich, Germany

[11] Institute for Theoretical Physics, University of Cologne, 50937, Köln, Germany

[12] Department of Environmental Sciences Faculty of Science, Open University, Heerlen, The Netherlands

[13] Faculty of Science and Technology, Norwegian University of Life Sciences, 1432 Ås, Norway

1 Introduction

Paleoclimate proxy records provide evidence for past abrupt climate shifts from regional to at least hemispheric scale (e.g. Menviel et al. 2020; Brovkin et al. 2021; Boers et al. 2022). Long-term climate simulations suggest that anthropogenic global warming could trigger structurally similar transitions in several Earth system components in the future, i.e., that these components could 'tip' to a qualitatively different state (e.g. Lenton et al. 2008, 2019; Boers 2021; Armstrong et al. 2022; Boulton et al. 2022; Wang et al. 2023). Such catastrophic shifts would have severe consequences on societies and ecosystems and may even unleash feedbacks, further increasing the global mean temperature. However, the assessment of potentially upcoming tipping points is challenging as the capability of modern complex climate models to simulate climate tipping dynamics is still limited (Valdes 2011; Liu et al. 2017; Wang et al. 2023). In light of this, the study of past abrupt climate shifts may provide insights into the processes involved in climate tipping events. Furthermore, past events may serve as benchmarks for the performance of fully coupled models in simulating the non-linear and high-dimensional dynamics that could lead to tipping events. In this context, we reassess here two proxy time series from the NGRIP ice core (North Greenland Ice Core Projects members 2004), which feature pronounced imprints of abrupt climatic transitions, by means of the Kramers–Moyal equation.

Agnostic time series models, i.e., models whose dynamics appear to reproduce nature but are not entirely based on physical mechanisms, have played a major role in furthering the debate on climate tipping phenomena (e.g. Riechers et al. 2023a; Boers et al. 2017; Mitsui and Crucifix 2017; Kwasniok 2013; Lohmann and Ditlevsen 2018; Dakos et al. 2008; Bochow and Boers 2023). The ability to produce quantitatively similar dynamical behaviour building only on heuristic physical assumptions facilitates the statistical analysis of tipping phenomena, employing methods of stochastic analysis (Lenton et al. 2012; Morr and Boers 2024; Morr et al. 2024). The common concept of a climate tipping element is that of a dynamical system whose current stable equilibrium state is prone to annihilation in a dynamic bifurcation (Scheffer et al. 2009; Ashwin et al. 2012; Boers et al. 2022). This typically involves the reduction of complex, high-dimensional dynamics to just a few (if not one) summary observables that may be modelled in terms of stochastic differential equations (SDEs), i.e., as random dynamical systems. Therein, the noise term reflects the action of the unresolved dynamics on the summary observable (Hasselmann 1976). A common choice is to force the resolved variables with Gaussian white noise, but this approach may be overly simplistic in many situations. In particular, in the context of climate tipping points, a deviation from Gaussian white noise has important implications for the detection of early warning signals and for the probability of premature noise-induced tipping (Ditlevsen 1999; Lucarini et al. 2022; Benson et al. 2024; Kuehn ey al. 2022; Morr and Boers 2024).

Here, we investigate the famous heavy-oxygen δ^{18}O record from the NGRIP ice core (North Greenland Ice Core Projects members 2004). The data shows that repeated decadal-scale warming events of regionally up to 16 °C in amplitude, known as Dansgaard–Oeschger events, punctuated the North Atlantic climate throughout the last glacial interval (Dansgaard et al. 1984; Broecker et al. 1985; Johnsen et al. 1992; Dansgaard et al. 1993; Kindler et al. 2014). The sudden temperature increases were followed by a phase of moderate cooling before the temperatures ultimately relaxed back to colder levels in a second phase of more abrupt cooling. The two distinct cold and mild regimes are termed stadials and interstadials, respectively.

In line with the SDE approach outlined above, we regard the δ^{18}O and dust concentration records as realisations of one-dimensional Markov processes and estimate the corresponding KM coefficients (Tabar 2019). The two records exhibit concomitant shifts, which are interpreted as sudden adjustments of global mean temperature and reorganisations of the atmospheric circulation of at least hemispheric scale (Fuhrer et al. 1999; Ruth et al. 2003, 2007; Schüpbach et al. 2018). Previous studies have motivated through statistical means the employment of a Markovian framework for these dynamics Riechers et al. (2023b); Kwasniok (2013). There have also been conceptual arguments of time-scale separation that lend this framework credence Gottwald (2021); Riechers et al. (2024). Under this modelling assumption, the KM coefficients are closely related to the Fokker–Planck equation of time-evolving diffusive systems. We estimate from the data and subsequently compare the two Kramers–Moyal expansions with respect to their implied stochastic model structure. Specifically, we investigate whether the dynamics can each be represented by a canonical Langevin approach or whether a discontinuous noise component, such as Poisson jump diffusion, is needed.

This article is structured as follows: In Sec. 2 we briefly introduce the two paleo-climatic proxies that we examine. Subsequently, in Sec. 3, we detail the Kramers–Moyal expansion in one dimension as the prime method to construct time series models including noise and possibly discontinuous elements. Section 4 presents the results of this analysis: Herein, we show the mono- and bistability of the obtained models of the two records and discuss the need to choose a noise model different from Gaussian white noise.

In Sec. 5 we discuss our findings and relate them to previous work. Sec. 6 summarises our key findings and draws conclusions.

2 Data and pre-processing

This work relies on the δ^{18}O and dust concentration records obtained by the North Greenland Ice Core Project (NGRIP) (Ruth et al. 2003; North Greenland Ice Core Projects members 2004; Gkinis et al. 2014). From 1404.75 m to 2426.00 m of depth the joint record is provided at 5 cm equidistant resolution. This translates to the time span from 59945 yr to 10276 yr b2k (before 2000 CE) with ~ 5 yr resolution for the oldest and sub-annual resolution for the most recent part of the record (Fig. 1a and b). For the analysis, the data was rescaled, binned to an equidistant time axis of 5-year resolution, detrended, and normalised (see Appendix A for details).

The concentration of dust, i.e., the number of particles with a diameter larger than 1 μm per ml, is commonly interpreted as a proxy for the state of the hemispheric atmospheric circulation (e.g. Fischer et al. 2007; Ruth et al. 2007; Schüpbach et al. 2018; Erhardt et al. 2019). In particular, the dust storm activity and dryness over East Asian desserts, the strength and position of the polar jet, and local precipitation patterns govern the emission, transport, and deposition of the dust, respectively (Fischer et al. 2007; Erhardt et al. 2019). Correspondingly, the substantial changes in the dust concentrations at DO events are interpreted as large-scale reorganisations of the Northern Hemisphere's atmospheric circulation. In agreement with a widespread convention, we rescale the dust record by taking the net negative logarithm (e.g. Ditlevsen 1999; Mitsui and Crucifix 2017; Boers et al. 2017; Riechers et al. 2023a). In this form, the dust record exhibits a high degree of correlation with the δ^{18}O record (Boers et al. 2017).

In order to reduce the influence of slow changes in the background climate, we restricted the analysis to the period 59–27 kyr b2k and applied further detrending with respect to a Northern Hemisphere temperature reconstruction provided by Snyder (2016) (see Fig. 1c and d and App. Appendix A). The concentration of stable water isotopes expressed as δ^{18}O values in units of permil is a proxy for the site temperature at the time of precipitation (Jouzel et al. 1997; Gkinis et al. 2014).

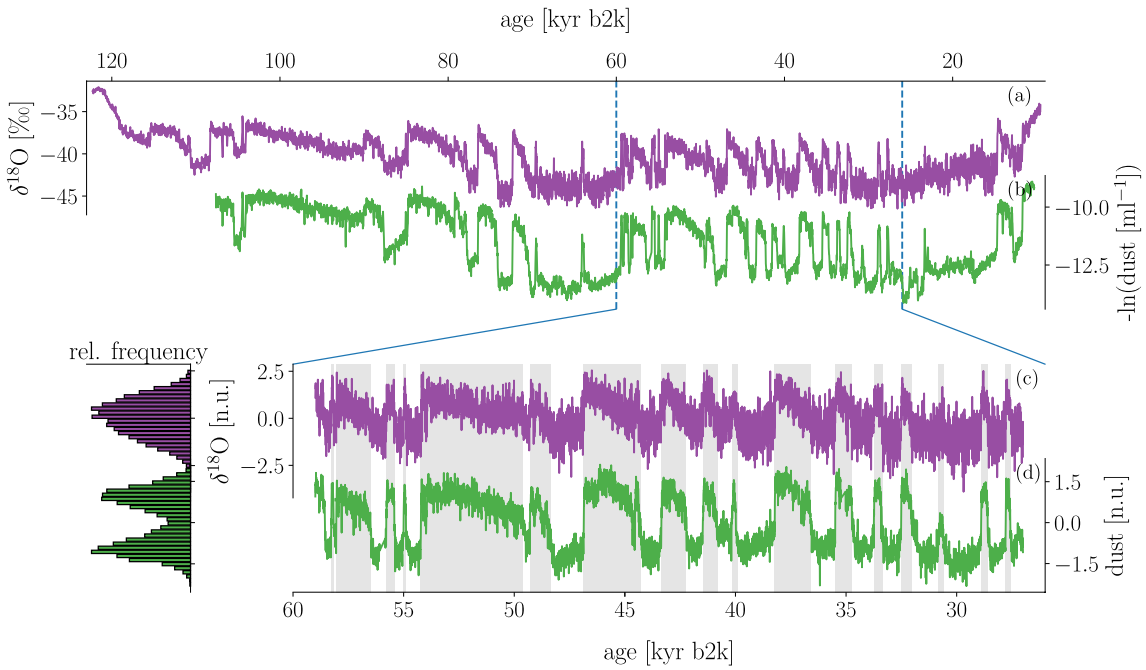

Fig. 1 Trajectories of the 20-year mean of δ^{18}O (**a**) and accordingly resampled dust concentrations (**b**) from the NGRIP ice core in Greenland, from 122 kyr and 107 kyr to 10 kyr before 2000 CE (b2k), respectively (Ruth et al. 2003; Rasmussen et al. 2014; Seierstad et al. 2014). The dust data is given as the negative natural logarithm of the actual dust concentrations, in order to facilitate comparison to the δ^{18}O data. Panels (**c**) and (**d**) show the same proxies but at a higher resolution of 5 years (North Greenland Ice Core Projects members 2004; Gkinis et al. 2014; Ruth et al. 2003) and over the shorter period from 59 to 27 kyr b2k. The analysis presented in this study was constrained to this segment of the records. The two proxy time series in (**c**) and (**d**) have been detrended by linearly regressing the data against reconstructed global mean surface temperatures (Snyder 2016) and removing the apparent background-temperature-driven slow change. The grey shadings mark the Greenland interstadial (GI) intervals according to (Rasmussen et al. 2014). All data are shown on the GICC05 chronology (Vinther et al. 2006; Rasmussen et al. 2006; Andersen 2006; Svensson et al. 2008). The data were binned to equidistant time resolution from its original 5 cm depth resolution (see App. Appendix A for further details on the data processing (Riechers et al. 2023a))

3 Methods

Our starting point is a (time-homogeneous) Markov stochastic process x_t of the form

$$\mathrm{d}x_t = f(x_t)\mathrm{d}t + \sigma(x_t)\mathrm{d}\xi_t, \tag{1}$$

where $\mathrm{d}\xi_t$ denotes an arbitrary uncorrelated stochastic force. The temporal evolution of the associated conditional probability function $p(x, t+\tau|x', t)$ then follows the Kramers–Moyal equation (Kramers 1940; Moyal 1949; Kampen 1961; Gardiner 2009; Risken and Frank 1996; Tabar 2019):

$$\frac{\partial}{\partial\tau}p(x,t+\tau|x',t) = \sum_{m=1}^{\infty}\left(-\frac{\partial}{\partial x}\right)^m D_m(x)\,p(x,t+\tau|x',t). \tag{2}$$

The Kramers–Moyal (KM) coefficients $D_m(x)$ are related to the conditional moments $M_m(x,\tau)$ of order m of the stochastic variable x at a time-lag τ by

$$\begin{aligned} D_m(x) &= \frac{1}{m!}\lim_{\tau\to 0}\frac{1}{\tau}M_m(x,\tau) \\ &= \frac{1}{m!}\lim_{\tau\to 0}\frac{1}{\tau}\int (x'-x_t)^m p(x',t+\tau|x,t)\mathrm{d}x'. \end{aligned} \tag{3}$$

In the special case that the stochastic force in Eq. (1) is given by Gaussian white noise (i.e., it can be expressed by the increments of a Wiener process W_t), only the first two terms on the right of Eq. (2) contribute and the Kramers–Moyal equation reduces to the better-known Fokker–Planck equation (Fokker 1913, 1914; Planck 1917). With $\mathrm{d}\xi_t = \mathrm{d}W_t$, Eq. (1) becomes the Langevin equation and the resulting process is then referred to as a Langevin process[1]. For Langevin processes the relation

$$D_1(x) = f(x) \quad \text{and} \quad D_2(x) = \frac{1}{2}\sigma^2(x), \tag{4}$$

between the KM coefficients, the drift $f(x)$ and the diffusion $\sigma(x)$, holds in general.

The other way around, if higher-order moments contribute to the Kramers–Moyal equation, the underlying process cannot be a standard Langevin process. In that case, ξ_t does not correspond to a Wiener process but has instead a more complex form. However, the first two KM coefficients would still be dominated by the process' drift and diffusion.

While a Langevin process consists, with probability 1, of continuous sample paths (e.g. Theorem 5.1.1 in Arnold 1974), a Markov stochastic process of the form Eq. (1) generally features discontinuous paths with non-zero probability. Path-wise continuity is only one of many notions of continuity in stochastic processes. Another is the continuity criterion for Markov processes provided by Gardiner (2009), which requires for a process to be continuous that

$$\begin{aligned} C(x,t,\delta) &= \lim_{\tau\to 0}\frac{1}{\tau}P\left(|x_{t+\tau}-x_t|>\delta\right) \\ &= \lim_{\tau\to 0}\frac{1}{\tau}\int\limits_{|x'-x|>\delta} p(x',t+\tau|x,t)dx' \overset{!}{=} 0, \end{aligned} \tag{5}$$

for all δ, x, and t. In words, this means that the probability of a particle deviating from a reference position more than δ in a time interval τ decreases faster than linearly with τ. The presence of higher-order KM coefficients in the corresponding Kramers–Moyal equation is a necessary, yet not sufficient criterion for a given process to be discontinuous under this latter notion.

3.1 Estimating Kramers–Moyal coefficients

The central entry point for this work is Eq. (3). It provides a means to estimate the KM coefficients $D_m(x)$ directly from data, i.e., from a recorded realisation of a stochastic process, provided that the following assumptions are fulfilled (to a reasonable degree):

i) The observed process is a Markov process,
ii) the process is time-homogeneous, i.e., the dynamics did not change over time,
iii) the state space is sampled sufficiently densely,
iv) and the sampling time is short compared to the characteristic time scale of the dynamics.

Under these conditions, the evaluation of the conditional statistical moments $M(x,\tau)$ at the shortest available time lag Δt given by the sampling rate yields a good estimate for the KM coefficients:

$$\hat{D}_m(x) = \frac{1}{m!}\frac{1}{\Delta t}\langle (x_{t+\Delta t}-x_t)^m\,|_{x_t=x}\rangle \approx D_m(x), \tag{6}$$

wherein the ensemble average in Eq. (3) is replaced by the average over the available data $\langle\cdot\rangle$. Our numerical implementation of Eq. (6) is based on the Nadaraya–Watson estimator which is detailed in App. Appendix B.

[1] There is no agreement on the use of the term Langevin process. Some authors consider Lévy-driven equations as such Langevin equations, others prefer to refer to Langevin processes as those that are solely driven by Gaussian/Brownian noise.

3.2 Estimators of discontinuous motion

Once the KM coefficients are estimated from the data, one can draw inference on the most fitting choice of the noise model $\mathrm{d}\xi_t$. Vanishing higher-order moments ($m > 2$) classify the model as a Langevin process. In contrast, demonstrable contributions of these moments suggest that the process is best modelled by including noise beyond a Wiener process (see e.g. Kampen 1961; Van Kampen 2007; Gardiner 2009; Tabar 2019; Lin 2023).

The finite sampling time step Δt introduces a bias for the estimators $\hat{D}_m(x)$ (Kurth et al. 2021). As a consequence, even for a Langevin process the expected values for the higher-order KM estimators differ from zero. A first pragmatic metric to discern whether a studied process is a Langevin process or not is to evaluate the ratio between the fourth KM coefficient and the second, i.e., $D_4(x)/D_2(x)$. This gauges the distributional tail of all immediate disturbances originating from x. It therefore offers a non-parametric insight into whether a fat tail of disturbances is needed to recreate the dynamics at the considered sampling rate. Such conclusions would be largely model-independent and do not explicitly rely on the Markovianity of the data. Small values $\lesssim 0.1$ are typically regarded as a justification for a Langevin description. Values $D_4(x)/D_2(x) \gtrsim 0.1$ point to non-diffusive motion (i.e., forcing beyond Gaussian white noise). This metric offers a first insight into whether a discontinuous noise term ξ_t is needed to model the process (Gao et al. 2016; Lu and Duan 2020; Lucarini et al. 2022).

When the Langevin process model is contrasted with a jump-diffusion model of the form (Tabar 2019; Lin 2023)

$$\mathrm{d}x_t = f(x_t)\mathrm{d}t + \sigma(x_t)\mathrm{d}W_t + \eta(x_t)\mathrm{d}J_t^{(\lambda)}, \tag{7}$$

the assessment can be further refined. Here, $J_t^{(\lambda)}$ denotes a Poissonian jump process characterised by the rate λ. The jump amplitude is determined by the Gaussian stochastic variable $\eta(x)$. For this specific process model, the KM coefficients read (Tabar 2019)

$$\begin{aligned} D_1(x) &= f(x), \\ D_2(x) &= \frac{1}{2}\sigma(x)^2 + \frac{1}{2}\lambda(x)\langle\eta(x)^2\rangle, \\ D_m(x) &= \frac{1}{m!}\lambda(x)\langle\eta(x)^m\rangle, \ \text{for } m > 2, \end{aligned} \tag{8}$$

where $\langle\cdot\rangle$ expresses the expected value.

Similarly, the bias of the KM estimators defined by Eq. (6), when applied to a jump-diffusion process sampled at finite time step Δt, can be derived analytically. These considerations offer two additional metrics to distinguish Langevin from jump-diffusion processes, namely the Θ -ratio

$$\Theta(x,\tau) = \frac{3M_2(x,\tau)^2}{M_4(x,\tau)} \sim \begin{cases} 1, & \text{Langevin,} \\ \frac{1}{\tau}, & \text{jump-diffusion,} \end{cases} \tag{9}$$

and the Q-ratio (Lehnertz et al. 2018)

$$Q(x,\tau) = \frac{M_6(x,\tau)}{5M_4(x,\tau)} \sim \begin{cases} \tau, & \text{Langevin,} \\ \text{constant,} & \text{jump-diffusion.} \end{cases} \tag{10}$$

For details on the derivation of these relationships, we refer the interested reader to (Tabar 2019). Observing either of the scalings given in Eqs. (9) and (10), respectively, can aid in deciding between employing a Langevin or jump-diffusion model.

These relationships are specifically derived for the jump-diffusion model. Compared to the ratio of D_4 and D_2 discussed above, the results here are more prone to invalidity due to unjustified modelling assumptions on the real data. For different noise models than the ones introduced above, different scaling behaviours of these ratios with respect to τ will arise. Data from, e.g., a non-Markovian system may, on the other hand, exhibit the described behaviour while actually harbouring entirely different internal dynamics. In this work, we focus on distinguishing between the Langevin and Poisson jump-diffusion models as two archetypical (dis-) continuous stochastic models. Observing any other scaling in Q or Θ may hint at a third model being more appropriate to reproduce the time series dynamics. However, in the context of continuous versus discontinuous stochastic models, considering the two discussed models yields essential information.

4 Results

Figure 2 shows the first and second KM coefficients, and the ratio of the second to the fourth KM coefficients, as estimated from the dust and δ^{18}O time series according to Eq. (6). The corresponding Θ and Q ratios are presented in Fig. 3.

a Dust record: For the dust, the constructed drift $D_1(x)$ in Fig. 2b exhibits two separate stable states that match the maxima of the probability density function in Fig. 2a. The second KM coefficient $D_2(x)$ in Fig. 2c is approximately constant. The ratio between the fourth and the second KM coefficients in Fig. 2d is smaller than 0.1 on the entire state space probed by the time series. For large portions of the dust's state space, we find in Fig. 3 a decrease of the $\Theta(x,\tau)$ ratio with increasing τ, similar to a $1/\tau$ behaviour. This applies, in particular, at the stable equilibria of the drift,

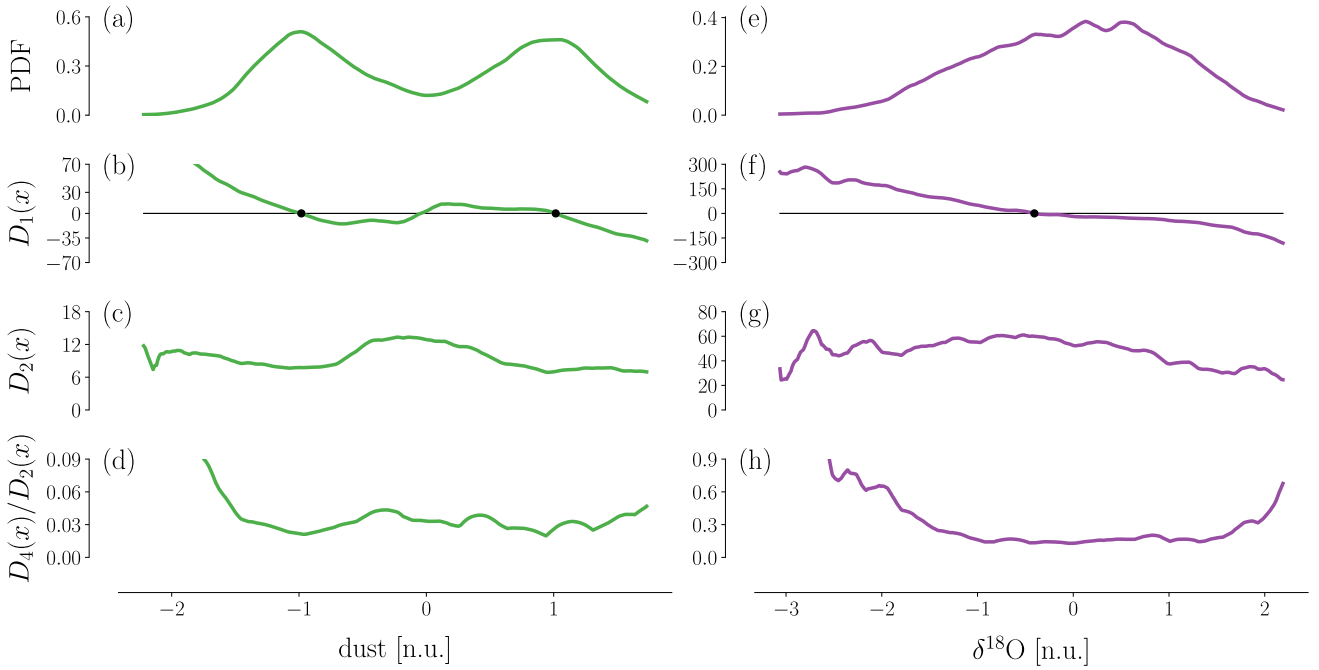

Fig. 2 The probability density function (PDF) of (**a**) the dust and (**e**) δ^{18}O. The non-parametric estimates of the (**b**, **f**) first KM coefficient $D_1(x)$ and (**c**, **g**) the second KM coefficient $D_2(x)$. The ratio between the fourth and the second KM coefficient $D_4(x)/D_2(x)$ (**d** and **h**). All KM coefficients are evaluated at the shortest available time step $\Delta t = 5$yr of the time series. The estimated dust drift is bistable, while that of δ^{18}O is monostable. The second KM coefficient $D_2(x)$ is relatively constant for both records. The ratio $D_4(x)/D_2(x)$ is small ($\lesssim 0.1$) for the dust record. Yet, it is non-negligible for δ^{18}O ($\gtrsim 0.3$) in large parts of the state space, suggesting that the driving noise in a stochastic model for these time series should not be exclusively Gaussian white noise. Details on the choice of kernel and bandwidth used for the KM coefficient estimation, as well as an analysis of the influence of the kernel bandwidth, can be found in App. B

where the data availability is the best and our estimation is most robust. The dust $\Theta(x,\tau)$-ratio is close to 1 only in a region of its state space where its probability density has a local minimum ($-0.3 \lesssim \text{dust} \lesssim 0.3$). The corresponding $Q(x,\tau)$-ratio shows quite a distinct linear increase with increasing τ – at least for small values of τ. For larger values of τ, $Q(x,\tau)$ is constant.

b δ^{18}Orecord: In the case of δ^{18}O, the drift has only one zero-crossing. This seems to explain the unimodal distribution of the data, though this broader distribution could also be caused by larger observational noise in the record. The mono-stability of the drift would not be affected by time- and state-independent observational noise and can therefore be seen as a more direct insight into the potential underlying dynamics. We note that NGRIP data products that provide δ^{18}O concentrations at a lower time resolution of 20- or 50-year time steps exhibit a bimodal distribution. For the purposes of our analysis, however, only the highest available sampling rate of time series data should be used so as to curtail the biases incurred in the KM estimations. With respect to the normalised units, the first and second KM coefficients of δ^{18}O exceed their counterparts for dust by factors of approximately 4 and 10, respectively. This indicates that δ^{18}O was subjected to stronger noise while simultaneously stronger deterministic forces acted on the variable. Finally, the ratio $D_4(x)/D_2(x) \gtrsim 0.3$ is 10 times larger for δ^{18}O than for the dust. The δ^{18}O record exhibits a mostly constant $\Theta(x,\tau)$-ratio with respect to τ, as seen in Fig. 3. It is slightly below but still close to 1 for large parts of the state space. The corresponding $Q(x,\tau)$-ratio is likewise constant (≈ 1) with respect to τ, with variations in both directions.

5 Discussion

The assessment of the KM coefficients and the scaling of Θ and Q ratios from the dust and the δ^{18}O records provides some insight into how to best model the proxy time series within the framework of one-dimensional stochastic processes.

For the dust, we find bistability of the estimated model's drift. The small $D_4(x)/D_2(x)$ ratio and the linear increase of the $Q(x,\tau)$ with increasing τ indicate that this process can, in fact, be modelled as a Langevin process. Only the assessment of the $\Theta(x,\tau)$ ratio calls this conclusion into question. For a Langevin process, this ratio should be equal to one, but we observe a $1/\tau$-like scaling for small values of τ, in line with an underlying jump-diffusion process.

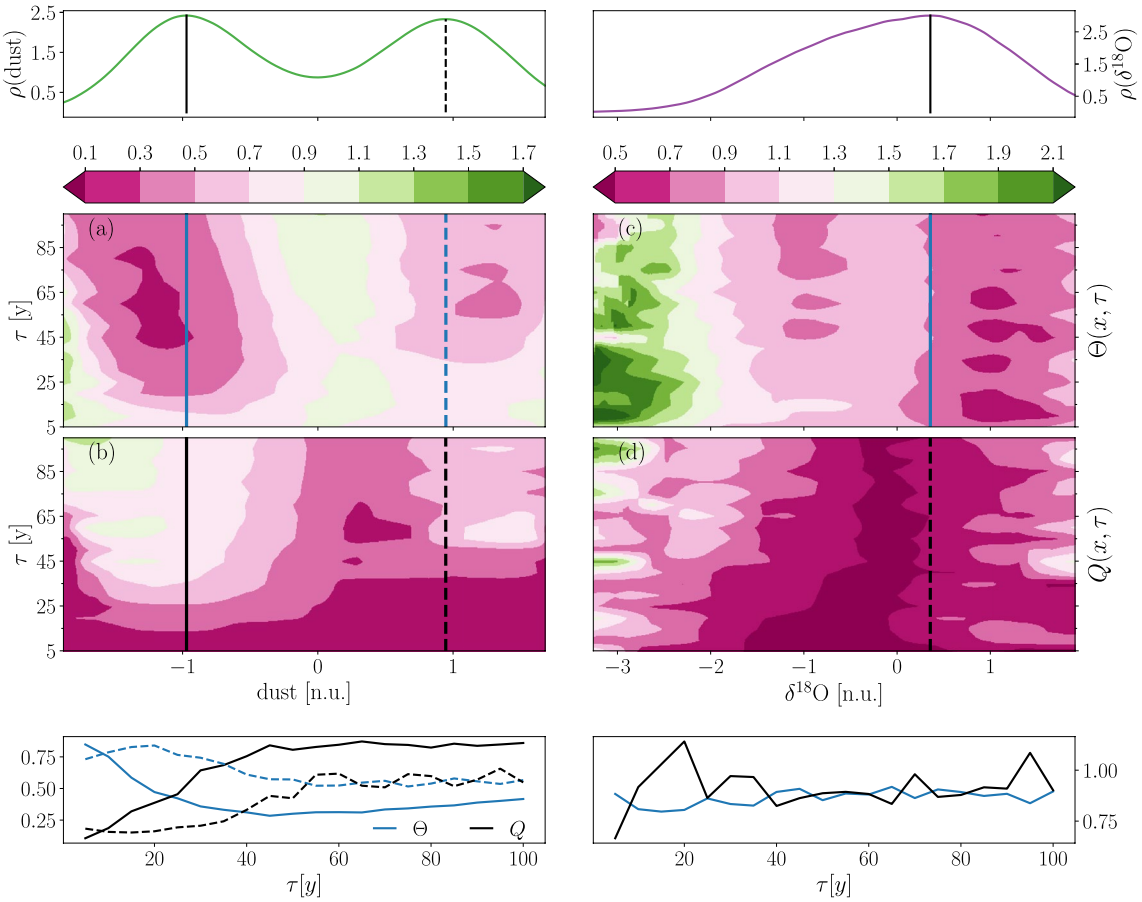

Fig. 3 The $\Theta(x,\tau)$-ratio and $Q(x,\tau)$-ratio of the dust and the δ^{18}O concentration. (a) The $\Theta(x,\tau)$-ratio of the dust is not close to 1 for a large range of τ and x, particularly around the peaks of the bimodal dust distribution. (b) From $\tau = 5$ to roughly $\tau = 50$ the $Q(x,\tau)$-ratio increases linearly with τ, consistent with a continuous process, yet for $\tau > 50$ the $Q(x,\tau)$-ratio is nearly constant, consistent with a discontinuous process. (**c**) On the one hand, the $\Theta(x,\tau)$-ratio of the δ^{18}O points to being different from 1 along the peak of the distribution, yet not sufficiently conclusive to ascertain if the δ^{18}O is discontinuous. (**d**) On the other hand, the $Q(x,\tau)$-ratio is arguably constant over τ, consistent with a discontinuous δ^{18}O. For visualisation purposes, $Q(x,\tau)$ of δ^{18}O is multiplied by 0.6 to match the scale of $Q(x,\tau)$ of the dust (Harris et al. 2020; Virtanen et al. 2020; Rydin Gorjão and Meirinhos 2019; Rydin Gorjão et al. 2023; Hunter 2007)

We note that a simple Langevin model with a bistable drift and purely diffusive noise can produce the regime shifts observed in the dust record. However, such a model is unlikely to reproduce the asymmetric shape of the interstadial phases evident in the record.

For the δ^{18}O record, the results are exactly the opposite. The constructed drift function exhibits only a single stable equilibrium. The observed quantities $D_4(x)/D_2(x)$ and $Q(x,\tau)$ provide evidence for relevant contributions from higher-order KM coefficients. The $\Theta(x,\tau)$ ratio, however, is close to one in agreement with a Langevin model. A Langevin model together with the evidenced single equilibrium of the drift function clearly fails to explain the two regimes of the δ^{18}O record, and the apparent time asymmetry. Taken together, we conclude that the evidence speaks in favour of introducing discontinuities to the driving noise model rather than against it. Complex noise, i.e., noise beyond a Wiener process, could indeed be a way to reproduce time series with two regimes in the presence of a single equilibrium and time asymmetry (Chechkin et al. 2003, 2004; Metzler and Klafter 2004; Yang et al. 2020).

Given the high degree of visual similarity between the dust and the δ^{18}O records, the differences in the reconstructed potentials and the ratio between the fourth and the second KM coefficient are remarkable. This accentuates the need for careful statistical analysis when devising time series models for non-linear systems with abrupt transitions.

Adopting a generalised Langevin equation with a bistable drift term, Ditlevsen (Ditlevsen 1999) showed that the noise in the calcium concentration record from the GRIP ice core can be modelled with an α-stable component. Calcium concentrations are typically considered equivalent to dust concentrations (cf. (Fuhrer et al. 1993; Ruth et al. 2002, 2003; Fischer et al. 2007)). We cannot directly assess the presence of α-stable noise in the NGRIP dust record. This is because noise models with infinite statistical moments, which can

be found in α-stable distributions, are inherently incompatible with the Kramers–Moyal framework. Yet, our results corroborate the notion that Greenland ice core records bear the signature of non-Gaussian noise, though in our analysis this arises primarily for the δ^{18}O record. Related to this, Gottwald (2020) recently formulated a conceptual model of DO events wherein α-stable noise plays a central role as an event trigger, later extended by Riechers et al. (2023a). From the perspective of theoretical stochastic modelling, it is worth noting that the α-stable noise model leads to a pathwise continuous process, in contrast to the Poisson jump-diffusion model discussed in this work. Employing the continuity notion of Eq. (5), however, both of these models would be considered discontinuous.

We have to state that the interpretation of higher-order KM coefficients is not straightforward and depends on the exact choice of the stochastic model. A direct causal relation between the DO events and discontinuous noise cannot be inferred without further ado within this study, but the role of discontinuities in the proxy records merits further investigation. It has been observed in complex model simulations that (stochastic) atmospheric anomalies can indeed drive regime changes in the North Atlantic region (Drijfhout et al. 2013; Kleppin et al. 2015). Together with the apparent aptitude of non-Gaussian noise models for Greenland temperature and Northern Hemisphere atmospheric circulation proxies, this motivates further research on the effect that non-Gaussian noise could have on climate tipping elements in present-day climate.

If both Greenland temperatures and the state of the Northern Hemisphere atmospheric circulation were subject to non-Gaussian noise, and if indeed pulses of this noise triggered transitions between stadial and interstadial regimes, this would have important implications for our conception of stability of certain climate tipping elements. The possibility that climate tipping elements are nowadays likewise subject to non-Gaussian stochastic forcing warrants more attention.

6 Conclusion

In this work, we presented a data-driven analysis of the δ^{18}O and dust concentration records from the NGRIP ice core, based on the Kramers–Moyal equation. This equation generalises the Fokker–Planck equation by allowing for arbitrarily complex uncorrelated driving noise $\mathrm{d}\xi_t$. In particular, such noise may result in a discontinuous process.

The estimation of the KM coefficients yielded a monostable drift for the isolated δ^{18}O record and a bistable one for the dust. The analysis of the resulting agnostic time series models does not allow for conclusions about the dynamical stability of the actual physical processes. It is, however, notable that these findings are inconsistent with the hypothesis that past Greenland temperatures were governed by intrinsically bistable dynamics (Livina et al. 2010; Kwasniok 2013). For the atmospheric circulation, there is no such inconsistency. We stress that this inconsistency with respect to previous studies arises under the application of differing modelling assumptions and data pre-processing procedures. The potential influence of non-Markovianity in the dynamics or complex measurement noise cannot be quantified. Disentangling these confounding effects is possible but demands large amounts of data Böttcher et al. (2006). We nonetheless maintain that this novel perspective is a valuable data point for further conceptual and physical considerations of DO events.

We found that stochastic forcing should include terms beyond Gaussian white noise when modelling the δ^{18}O record. This renders the Langevin approach insufficient to accurately reproduce the time series characteristics, drawing attention towards including discontinuous elements. For the dust record, similar indications could be found, though these have not been as convincing.

In physical terms, complex noise could have played a central role in the emergence of DO events. Our analysis does not provide direct evidence for a causal relation between discontinuous driving noise and the regime switches of the North Atlantic region's climate during the last glacial. Yet, it motivates further exploration of this issue along the lines of Gottwald (2020) and Riechers et al. (2023a). The possibility that climate tipping elements are subject to non-Gaussian noise in today's climate should receive greater consideration. The corresponding implications on the stability of these elements and the ability to detect early warning signals should be investigated.

Appendix A: Data detrending

As mentioned in Sec. 2, this study focuses on the period 59–27 kyr b2k. Detrending of the data is necessary to ensure that the time series are time-homogeneous stationary processes, which is an underlying assumption for the Kramers–Moyal analysis performed in our investigation. To compensate for the influence of the background climate on the climate proxy records of dust and δ^{18}O, we remove a linear drift with respect to reconstructed global average surface temperatures (Snyder 2016) from both time series. Figure 4 illustrates the detrending scheme. Due to the two-regime nature of the time series, a simple linear regression would overestimate the temperature dependencies. Instead, we separate the data from Greenland stadials (GS) and Greenland interstadials (GI) and then minimise the expression

$$R^2 = \sum_{i=1}^{N} \left(X_{t_i} - a_X \Delta T(t_i) - \begin{cases} b_{\mathrm{GI}}, & \text{if } t_i \in \mathrm{GI} \\ b_{\mathrm{GS}}, & \text{if } t_i \in \mathrm{GS} \end{cases} \right)^2, \tag{A1}$$

with X either dust or δ^{18}O and with respect to the parameters a_X, b_{GI}, and b_{GS}. For a given time $t_i \in$ GS (GI) indicates that t_i falls into a stadial (interstadial) period. The resulting a_X is used to detrend the original data with respect to the temperature. The detrended data are subsequently normalised by subtraction of their mean and division by their standard deviation.

Appendix B: Nadaraya–Watson estimator of the KM coefficients and bandwidth selection

In order to carry out the estimation in Eq. (6) we map each data point in the corresponding state space to a kernel density and then take a weighted average over all data points

$$\begin{aligned} D_m(x) &\sim \frac{1}{m!}\frac{1}{\Delta t}\langle (x_{t+\Delta t} - x_t)^m |_{x_t = x} \rangle \\ &\sim \frac{1}{m!}\frac{1}{\Delta t}\frac{1}{N}\sum_{i=1}^{N-1} K(x - x_i)(x_{i+1} - x_i)^m. \end{aligned} \tag{B1}$$

Similarly to selecting the number of bins in a histogram, for a kernel-density estimation, we select both a kernel and a bandwidth (Nadaraya 1964; Watson 1964; Lamouroux and Lehnertz 2009). The kernel is a function $K(x)$ for the estimator $\widehat{f}_h(x)$, where h is the bandwidth at a point x, following

$$\widehat{f}_h(x) = \frac{1}{nh}\sum_{i=1}^{n} K\left(\frac{x - x_i}{h}\right) \tag{B2}$$

for a collection $\{x_i\}$ of n random variables. The kernel $K(x)$ is normalisable $\int K(x)\mathrm{d}x = 1$ and has a bandwidth h, such that $K(x) = K(x/h)/h$ (Rydin Gorjão et al. 2019; Tabar 2019; Davis and Buffett 2022). The bandwidth h is equivalent to the selection of the number of bins, except that binning in a histogram is always 'placing numbers into non-overlapping boxes'. We use an Epanechnikov kernel

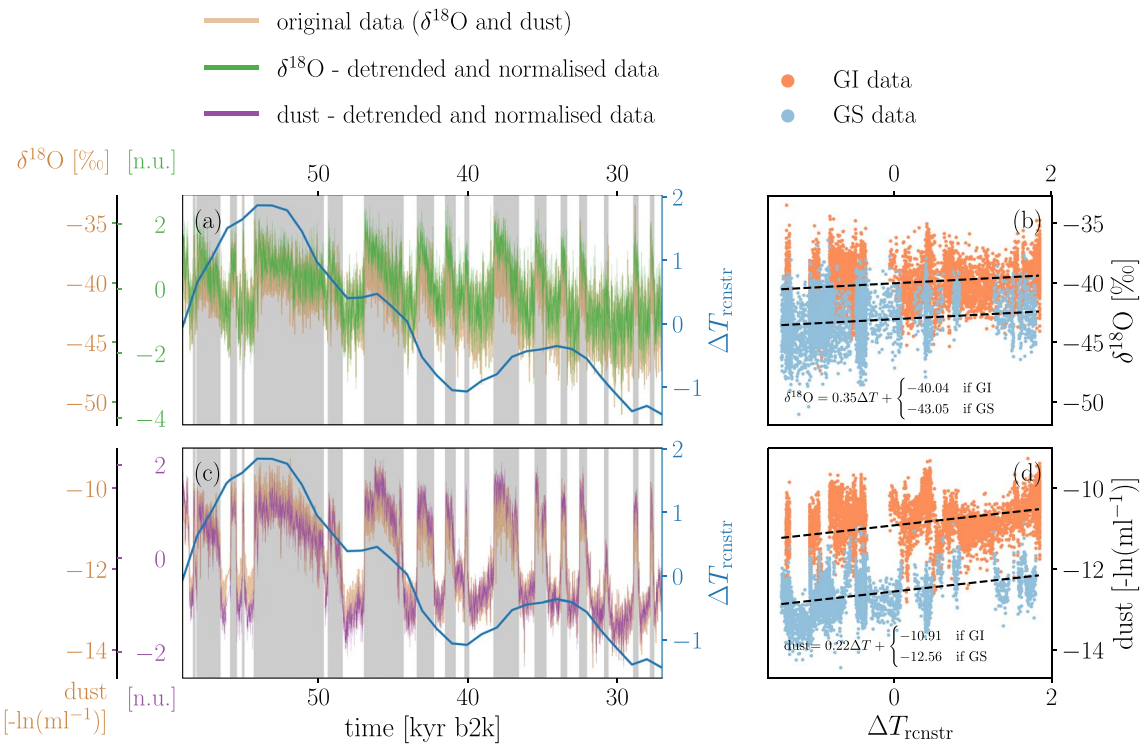

Fig. 4 Removal of a linear trend in the NGRIP δ^{18}O and dust time series (North Greenland Ice Core Projects members 2004) with respect to a global average surface temperature reconstruction (Snyder 2016). In panel (**a**) both original δ^{18}O (light brown) as well as detrended and normalised (purple) time series are shown. Likewise for the dust record in panel (**b**) (light brown and green, respectively). The background temperature is given in anomalies with respect to the mean over the investigated period (blue). Panels (**c**) and (**d**) show scatter plots of the original δ^{18}O and dust data with respect to temporarily corresponding temperature anomalies, respectively. Data from interstadials (stadials) is shown in orange (light blue). The black dashed lines correspond to the fitting scheme that uses a single slope but two different offsets to separately fit the stadial and interstadial data

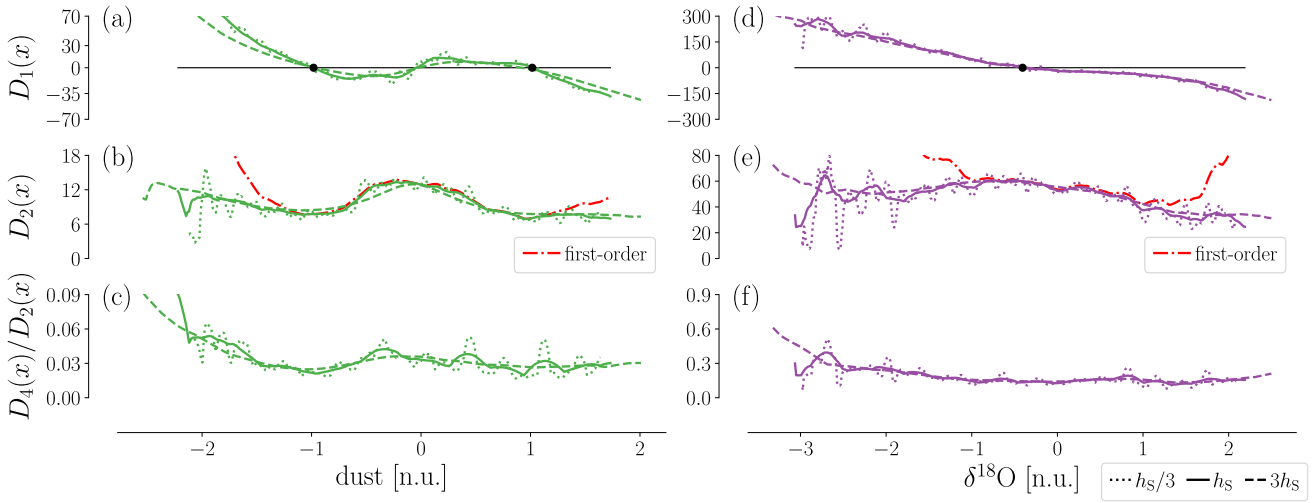

Fig. 5 The effect of the bandwidth selection h_S on the KM estimations, in similar fashion to Fig. 2. The non-parametric estimates of the first KM coefficient $D_1(x)$, the second KM coefficient $D_2(x)$, and the ratio of the fourth to the second KM coefficient $D_4(x)/D_2(x)$. Left column for dust, right column for δ^{18}O. Three bandwidths are used for the Nadaraya–Watson kernel-density estimator: the optimal Silverman's rule-of-thumb h_S, three times h_S, and one-third h_S. The Nadaraya–Watson kernel-density estimator's bandwidths h_S for δ^{18}O is 0.131 and for dust 0.103. In all cases, the interpretation of the estimator remains the same: bistability in the dust, mono-stability in the δ^{18}O. In (**b**) and (**e**) the first-order estimator for the second KM coefficient $D_2(x)$ are included, i.e., without corrective terms

$$K(x) = \frac{3}{4}(1-x^2), \text{ with support } |x| < 1, \tag{B3}$$

which has a compact bounded support, but other kernels are available, with different supports (Epanechnikov 1967). The selection of an appropriate bandwidth h follows Silverman's rule-of-thumb (Silverman 1998), given by

$$h_S = \left(\frac{4\hat{\sigma}^5}{3n}\right)^{\frac{1}{5}}, \tag{B4}$$

where σ^2 is the variance of the time series. In Fig. 5 three different bandwidths are used to evaluate the various KM coefficients, as given in Fig. 2. The bandwidths are the optimal bandwidth given by Silverman's rule-of-thumb h_S, three times h_S, and one-third h_S.

Note that regardless of the choice of bandwidth, the mono-stability of the δ^{18}O model is preserved, as is the bistability of the dust concentration model.

Appendix C: Understanding continuity and discontinuity in stochastic processes

The understanding of *continuity* and *discontinuity* can sometimes be unclear when dealing with time series data. We turn to Lindeberg's continuity condition $C(x,t,\delta)$ for a Markov process (Lehnertz et al. 2018; Tabar 2019), which states that a process x_t is continuous if

$$\begin{aligned} C(x,t,\delta) &= \lim_{\tau\to 0} \frac{\text{Prob}\left[\,|x_{t+\tau}-x_t| > \delta|_{x_t=x}\right]}{\tau} \\ &= \lim_{\tau\to 0} \frac{\int_{|x'-x|>\delta} p(x',t+\tau|x,t)\mathrm{d}x'}{\tau} \\ &= 0. \end{aligned} \tag{C1}$$

In words, this means that the probability of a particle deviating from a reference position more than δ in a time interval τ decreases faster than linearly with τ. Direct proof is easily obtained for some particular processes. For example, for a Brownian motion we obtain, as expected, $C(x,t,\delta) = 0$ (see (Tabar 2019), Eq. (4.5) for a derivation). In a similar fashion, Tabar (2019) also shows two examples where $C(x,t,\delta) > 0$. These are the Cauchy process (which is the special case of an α-stable Lévy-driven Langevin process with $\alpha = 1$) and processes with Poissonian jumps (see Eq. (4.6) and Eq. (11.19)). Both examples are discontinuous processes by this definition.

For discontinuous processes in our KM setting we can derive a relation similar in form to Lindeberg's continuity condition, namely $C(x,t,\delta) \leq \frac{\bar{M}_m(x)}{\delta^m}$. We follow almost verbatim the derivation by Tabar, S11.2 (Tabar 2019). Consider the *m*-th order conditional moment of the *absolute value* of the increment

$$\begin{aligned}\langle |x_{t+\tau} - x_t|^m |_{x_t=x} \rangle &= \langle |x' - x|^m |_{x_t=x} \rangle \\ &= \int_{-\infty}^{\infty} |x' - x|^m p(x', t+\tau | x, t) \mathrm{d}x' \\ &\geq \int_{|x'-x|>\delta} |x' - x|^m p(x', t+\tau | x, t) \mathrm{d}x',\end{aligned} \tag{C2}$$

where we disregarded the integration over the interval $[x-\delta, x+\delta]$, δ being a small value. Using further that $|x'-x|^m > \delta^m$, we get

$$\langle |x' - x|^m |_{x_t=x} \rangle \geq \delta^m \int_{|x'-x|>\delta} p(x', t+\tau | x, t) \mathrm{d}x'. \tag{C3}$$

Dividing both sides by τ and taking the limit $\tau \to 0$, we obtain

$$\lim_{\tau \to 0} \frac{1}{\tau} \delta^m \int_{|x'-x|>\delta} p(x', t+\tau | x, t) \mathrm{d}x' \leq \lim_{\tau \to 0} \frac{1}{\tau} \langle |x' - x|^m |_{x_t=x} \rangle, \tag{C4}$$

where we recognise the form of Lindeberg's continuity condition as

$$C(x, t, \delta) \leq \frac{\bar{M}_m(x)}{\delta^m}, \tag{C5}$$

with

$$\bar{M}_m(x) = \lim_{\tau \to 0} \frac{1}{\tau} \langle |x' - x|^m |_{x_t=x} \rangle, \tag{C6}$$

noting the absolute value in contrast with Eq. (3). Although the relation comprises only an upper bound for $C(x, t, \delta)$, it yields a convincing argument for the role of the higher-order KM coefficients and their relation with discontinuity.

Note that having any vanishing KM coefficient of order $m > 2$ is sufficient for the process to be continuous. For the case of non-vanishing KM coefficients of higher order, Pawula's theorem (Pawula 1967a, b; Risken and Frank 1996) implies that all KM coefficients exist. It is reasonable to expect Lindeberg's continuity condition will *not* be obeyed for at least one order m (note the left-hand side of Eq. (C5) does not depend on m). Consequently, higher-order KM coefficients relate to discontinuous trajectories. This, however, does not imply that the Kramers–Moyal equation is necessarily the only model – or even the best model – to describe discontinuous processes (cf. Van Kampen 2007; Gardiner 2009).

Acknowledgements We thank Peter Ditlevsen for the conversations and early remarks on this manuscript that helped improve its content.

Author Contributions All authors contributed to the study conception and design. KR and LRG conducted the formal analysis. KR, LRG, and AM wrote the first draft. All authors contributed to editing the draft. All authors read and approved the final manuscript.

Funding Open Access funding enabled and organized by Projekt DEAL. LRG and DW gratefully acknowledge support from the Helmholtz Association via the grant Uncertainty Quantification – From Data to Reliable Knowledge (UQ) with grant agreement no. ZT-I-0029. This work was performed by LRG as part of the Helmholtz School for Data Science in Life, Earth and Energy (HDS-LEE). NB acknowledges funding from the Volkswagen Foundation. Funded by the Deutsche Forschungsgemeinschaft (DFG, German Research Foundation), grant no. 491111487. This is ClimTip contribution #75. The ClimTip project has received funding from the European Union's Horizon Europe research and innovation programme under grant agreement No. 101137601. Views and opinions expressed are however those of the author(s) only and do not necessarily reflect those of the European Union or the European Climate, Infrastructure, and Environment Executive Agency (CINEA). Neither the European Union nor the granting authority can be held responsible for them.

Data availability The code used for this study will be made available by the authors upon request.
All ice core data can be obtained from the website of the Niels Bohr Institute of the University of Copenhagen (https://www.iceandclimate.nbi.ku.dk/data/); the detailed links are indicated below.
The original measurements of δ^{18}O and dust concentrations go back to (North Greenland Ice Core Projects members 2004) and (Ruth et al. 2003), respectively.
The 5 cm resolution δ^{18}O and dust concentration data together with corresponding GICC05 ages used for this study can be downloaded from https://www.iceandclimate.nbi.ku.dk/data/NGRIP_d18O_and_dust_5cm.xls (accessed 2025-01-07).
The δ^{18}O data shown in Fig. 1 with 20 yr resolution that cover the period 122-10 kyr b2k are available from https://www.iceandclimate.nbi.ku.dk/data/GICC05modelext_GRIP_and_GISP2_and_resampled_data_series_Seierstad_et_al._2014_version_10Dec2014-2.xlsx (accessed 2025-01-07) and were published in conjunction with the work by Rasmussen et al. (2014) and Seierstad et al. (2014).
The corresponding dust data, also shown in Fig. 1 covering the period 108–10 kyr b2k, can be retrieved from https://www.iceandclimate.nbi.ku.dk/data/NGRIP_dust_on_GICC05_20y_december2014.txt (accessed 2025-01-07).
The global average surface temperature reconstructions provided by Snyder (2016) and used here for the detrending were retrieve from https://static-content.springer.com/esm/art%3A10.1038%2Fnature19798/MediaObjects/41586_2016_BFnature19798_MOESM258_ESM.xlsx (accessed 2025-01-07).

Declarations

Conflict of interest The authors have no relevant financial or non-financial interests to disclose.

References

Andersen KK, Svensson A, Johnsen SJ, Rasmussen SO, Bigler M, Röthlisberger R, Ruth U, Siggaard-Andersen ML, Peder Steffensen J, Dahl-Jensen D, Vinther BM, Clausen HB (2006) The Greenland Ice Core Chronology 2005, 15–42 ka. Part 1: constructing the time scale. Quater Sci Rev 25:3246. https://doi.org/10.1016/j.quascirev.2006.08.002

Armstrong McKay DI, Staal A, Abrams JF, Winkelmann R, Sakschewski B, Loriani S, Fetzer I, Cornell SE, Rockström J, Lenton TM (2022) Exceeding 1.5°C global warming could trigger multiple climate tipping points. Science 377:eabn7950. https://doi.org/10.1126/science.abn7950

Arnold L (1974) Stochastic differential equations: theory and applications, dover books on mathematics. Dover Publications https://doi.org/10.1142/6453

Ashwin P, Wieczorek S, Vitolo R, Cox P (2012) Tipping points in open systems: Bifurcation, noise-induced and rate-dependent examples in the climate system. Philos Trans R Soc A Math Phys Eng Sci 370:1166. https://doi.org/10.1098/rsta.2011.0306

Benson V, Donges JF, Boers N, Hirota M, Morr A, Staal A, Vollmer J, Wunderling N (2024) Measuring tropical rainforest resilience under non-Gaussian disturbances. Environ Res Lett 19:024029. https://doi.org/10.1088/1748-9326/ad1e80

Bochow N, Boers N (2023) The South American monsoon approaches a critical transition in response to deforestation. Sci Adv 9:eadd9973. https://doi.org/10.1126/sciadv.add9973

Boers N (2021) Observation-based early-warning signals for a collapse of the Atlantic Meridional Overturning Circulation. Nat Clim Chang 11:680. https://doi.org/10.1038/s41558-021-01097-4

Boers N, Chekroun MD, Liu H, Kondrashov D, Rousseau D-D, Svensson A, Bigler M, Ghil M (2017) Inverse stochastic-dynamic models for high-resolution Greenland ice core records. Earth Syst Dyn 8:1171. https://doi.org/10.5194/esd-8-1171-2017

Boers N, Ghil M, Stocker T (2022) Theoretical and Paleoclimate evidence for abrupt transitions in the Earth system Environmental Research Letters (in revision)

Böttcher F, Peinke J, Kleinhans D, Friedrich R, Lind PG, Haase M (2006) Reconstruction of complex dynamical systems affected by strong measurement noise. Phys Rev Lett 97:090603. https://doi.org/10.1103/PhysRevLett.97.090603

Boulton CA, Lenton TM, Boers N (2022) Pronounced loss of Amazon rainforest resilience since the early 2000s. Nat Clim Chang 12:271. https://doi.org/10.1038/s41558-022-01287-8

Broecker WS, Peteet DM, Rind D (1985) Does the ocean-atmosphere system have more than one stable mode of operation? Nature 315:21. https://doi.org/10.1038/315021a0

Brovkin V, Brook E, Williams JW, Bathiany S, Lenton TM, Barton M, DeConto RM, Donges JF, Ganopolski A, McManus J, Praetorius S, Vernal A, Abe-Ouchi A, Cheng H, Claussen M, Crucifix M, Gallopín G, Iglesias V, Kaufman DS, Kleinen T, Lambert F, Leeuw S, Liddy H, Loutre M-F, McGee D, Rehfeld K, Rhodes R, Seddon AWR, Trauth MH, Vanderveken L, Yu Z (2021) Past abrupt changes, tipping points and cascading impacts in the Earth system. Nat Geosci 14:550. https://doi.org/10.1038/s41561-021-00790-5

Chechkin AV, Klafter J, Gonchar VY, Metzler R, Tanatarov LV (2003) Bifurcation, bimodality, and finite variance in confined Lévy flights. Phys Rev E 67:010102. https://doi.org/10.1103/PhysRevE.67.010102

Chechkin AV, Gonchar VY, Klafter J, Metzler R, Tanatarov LV (2004) Lévy Flights in a Steep Potential Well. J Stat Phys 115:1505. https://doi.org/10.1023/B:JOSS.0000028067.63365.04

Dakos V, Scheffer M, Nes EH, Brovkin V, Petoukhov V, Held H (2008) Slowing down as an early warning signal for abrupt climate change. Proc Natl Acad Sci 105:14308. https://doi.org/10.1073/pnas.0802430105

Dansgaard W, Johnsen SJ, Clausen HB, Dahl-Jensen D, Gundestrup NS, Hammer CU, Hvidberg CS, Steffensen JP, Sveinbjörnsdottir AE, Jouzel J, Bond G (1993) Evidence for general instability of past climate from a 250-kyr ice-core record. Nature 364:218. https://doi.org/10.1038/364218a0

Dansgaard W, Johnsen S, Clausen H, Dahl-Jensen D, Gundestrup N, Hammer C, Oeschger H (1984) North Atlantic climatic oscillations revealed by deep Greenland ice cores, in Climate Processes and Climate Sensitivity (American Geophysical Union, 1984) pp 288–298 https://doi.org/10.1029/GM029p0288

Davis W, Buffett B (2022) Estimation of drift and diffusion functions from unevenly sampled time-series data. Phys Rev E 106:014140. https://doi.org/10.1103/PhysRevE.106.014140

Ditlevsen PD (1999) Observation of α-stable noise induced millennial climate changes from an ice-core record. Geophys Res Lett 26:1441. https://doi.org/10.1029/1999GL900252

Drijfhout S, Gleeson E, Dijkstra HA, Livina V (2013) Spontaneous abrupt climate change due to an atmospheric blocking-Sea-Ice-Ocean feedback in an unforced climate model simulation. Proc Natl Acad Sci 110:19713. https://doi.org/10.1073/pnas.1304912110

Epanechnikov VA (1967) Non-parametric estimation of a multivariate probability density. Theory Probab Appl 14:153. https://doi.org/10.1137/1114019

Erhardt T, Capron E, Olander Rasmussen S, Schüpbach S, Bigler M, Adolphi F, Fischer H (2019) Decadal-scale progression of the onset of Dansgaard-Oeschger warming events. Clim Past 15:811. https://doi.org/10.5194/cp-15-811-2019

Fischer H, Siggaard-Andersen ML, Ruth U, Röthlisberger R, Wolff E (2007) Glacial/interglacial changes in mineral dust and sea-salt records in polar ice cores: sources, transport, and deposition. Rev Geophys 45:1. https://doi.org/10.1029/2005RG000192

Fokker A D (1913) Over Brown'sche bewegingen in het stralingsveld, en waarschijnlijkheids-beschouwingen in de stralingstheorie, Ph.D. thesis, University of Leiden (1913) http://ilorentz.org/history/proefschriften/sources/Fokker_1913.pdf

Fokker AD (1914) Die mittlere Energie rotierender elektrischer Dipole im Strahlungsfeld. Ann Phys 348:810. https://doi.org/10.1002/andp.19143480507

Fuhrer K, Wolff EW, Johnsen SJ (1999) Timescales for dust variability in the Greenland Ice Core Project (GRIP) ice core in the last 100,000 years. J Geophys Res Atmos 104:31043. https://doi.org/10.1029/1999JD900929

Fuhrer K, Neftel A, Anklin M, Maggi V (1993) Continuous measurements of hydrogen peroxide, formaldehyde, calcium and ammonium concentrations along the new grip ice core from summit, Central Greenland. Atmos Environ Part A Gener Top 27: 1873 https://doi.org/10.1016/0960-1686(93)90292-7

Gao T, Duan J, Kan X, Cheng Z (2016) Dynamical inference for transitions in stochastic systems with α-stable Lévy noise. J Phys A Math Theor 49:294002. https://doi.org/10.1088/1751-8113/49/29/294002

Gardiner C (2009) Stochastic methods: a handbook for the natural and social sciences, 4th edn. Springer-Verlag, Berlin Heidelberg

Gkinis V, Simonsen SB, Buchardt SL, White JW, Vinther BM (2014) Water isotope diffusion rates from the NorthGRIP ice core for the last 16,000 years - Glaciological and paleoclimatic implications.

Earth Planet Sci Lett 405:132. https://doi.org/10.1016/j.epsl.2014.08.022
Gottwald GA (2020) A model for Dansgaard-Oeschger events and millennial-scale abrupt climate change without external forcing. Clim Dyn 56:227. https://doi.org/10.1007/s00382-020-05476-z
Gottwald GA (2021) A model for Dansgaard-Oeschger events and millennial-scale abrupt climate change without external forcing. Clim Dyn 56:227. https://doi.org/10.1007/s00382-020-05476-z
Harris CR, Millman KJ, Walt SJ, Gommers R, Virtanen P, Cournapeau D, Wieser E, Taylor J, Berg S, Smith NJ, Kern R, Picus M, Hoyer S, Kerkwijk MH, Brett M, Haldane A, Fernández del Río J, Wiebe M, Peterson P, Gérard-Marchant P, Sheppard K, Reddy T, Weckesser W, Abbasi H, Gohlke C, Oliphant TE (2020) Array programming with NumPy. Nature 585:357. https://doi.org/10.1038/s41586-020-2649-2
Hasselmann K (1976) Stochastic climate models: Part I. Theory. Tellus Dyn Meteorol Oceanogr 28:473. https://doi.org/10.3402/tellusa.v28i6.11316
Hunter JD (2007) Matplotlib: a 2D graphics environment. Comput Sci Eng 9:90. https://doi.org/10.1109/MCSE.2007.55
Johnsen SJ, Clausen HB, Dansgaard W, Fuhrer K, Gundestrup N, Hammer CU, Iversen P, Jouzel J, Stauffer B, Steffensen J (1992) Irregular glacial interstadials recorded in a new Greenland ice core. Nature 359:311. https://doi.org/10.1038/359311a0
Jouzel J, Alley RB, Cuffey KM, Dansgaard W, Grootes P, Hoffmann G, Johnsen SJ, Koster RD, Peel D, Shuman CA, Stievenard M, Stuiver M, White J (1997) Validity of the temperature reconstruction from water isotopes in ice cores. J Geophys Res Oceans 102:26471. https://doi.org/10.1029/97JC01283
Kampen NG (1961) A power series expansion of the master equation. Can J Phys 39:551. https://doi.org/10.1139/p61-056
Kindler P, Guillevic M, Baumgartner M, Schwander J, Landais A, Leuenberger M (2014) Temperature reconstruction from 10 to 120 kyr b2k from the NGRIP ice core. Clim Past 10:887. https://doi.org/10.5194/cp-10-887-2014
Kleppin H, Jochum M, Otto-Bliesner B, Shields CA, Yeager S (2015) Stochastic atmospheric forcing as a cause of Greenland climate transitions. J Clim 28:7741. https://doi.org/10.1175/JCLI-D-14-00728.1
Kramers HA (1940) Brownian motion in a field of force and the diffusion model of chemical reactions. Physica 7:284. https://doi.org/10.1016/S0031-8914(40)90098-2
Kuehn C, Lux K, Neamţu A (2022) Warning signs for non-Markovian bifurcations: colour blindness and scaling laws. Proc R Soc A Math Phys Eng Sci 478:20210740. https://doi.org/10.1098/rspa.2021.0740
Kurth JG, Rings T, Lehnertz K (2021) Testing jump-diffusion in epileptic brain dynamics: impact of daily rhythms. Entropy 23:309. https://doi.org/10.3390/e23030309
Kwasniok F (2013) Analysis and modelling of glacial climate transitions using simple dynamical systems. Philos Trans R Soc A Math Phys Eng Sci 371:20110472. https://doi.org/10.1098/rsta.2011.0472
Lamouroux D, Lehnertz K (2009) Kernel-based regression of drift and diffusion coefficients of stochastic processes. Phys Lett A 373:3507. https://doi.org/10.1016/j.physleta.2009.07.073
Lehnertz K, Zabawa L, Tabar MRR (2018) Characterizing abrupt transitions in stochastic dynamics. New J Phys 20:113043. https://doi.org/10.1088/1367-2630/aaf0d7
Lenton T, Held H, Kriegler E, Hall JW, Lucht W, Rahmstorf S, Schellnhuber HJ (2008) Tipping elements in the Earth's climate system. Proc Natl Acad Sci 105:1786. https://doi.org/10.1073/pnas.0705414105
Lenton TM, Livina VN, Dakos V, Nes EH, Scheffer M (2012) Early warning of climate tipping points from critical slowing down: comparing methods to improve robustness. Philos Trans R Soc A Math Phys Eng Sci 370:1185. https://doi.org/10.1098/rsta.2011.0304
Lenton TM, Rockström J, Gaffney O, Rahmstorf S, Richardson K, Steffen W, Schellnhuber HJ (2019) Climate tipping points - too risky to bet against. Nature 575:592. https://doi.org/10.1038/d41586-019-03595-0
Lin PP (2023) Characterization of jump-diffusion stochastic dynamics: analysis and applications on real world data, Ph.D. thesis, Universität Oldenburg https://oops.uni-oldenburg.de/id/eprint/5801
Liu W, Xie SP, Liu Z, Zhu J (2017) Overlooked possibility of a collapsed Atlantic meridional overturning circulation in warming climate. Sci Adv 3:e1601666. https://doi.org/10.1126/sciadv.1601666
Livina VN, Kwasniok F, Lenton TM (2010) Potential analysis reveals changing number of climate states during the last 60 kyr. Clim Past Discuss 5:2223. https://doi.org/10.5194/cpd-5-2223-2009
Lohmann J, Ditlevsen PD (2018) A consistent statistical model selection for abrupt glacial climate changes. Clim Dyn 52:6411. https://doi.org/10.1007/s00382-018-4519-2
Lu Y, Duan J (2020) Discovering transition phenomena from data of stochastic dynamical systems with Lévy noise. Chaos Interdiscip J Nonlinear Sci 30:093110. https://doi.org/10.1063/5.0004450
Lucarini V, Serdukova L, Margazoglou G (2022) Lévy noise versus Gaussian-noise-induced transitions in the Ghil-Sellers energy balance model. Nonlinear Process Geophys 29:183. https://doi.org/10.5194/npg-29-183-2022
Menviel LC, Skinner LC, Tarasov L, Tzedakis PC (2020) An ice-climate oscillatory framework for Dansgaard-Oeschger cycles. Nature Rev Earth Environ 1:677. https://doi.org/10.1038/s43017-020-00106-y
Metzler R, Klafter J (2004) The restaurant at the end of the random walk: recent developments in the description of anomalous transport by fractional dynamics. J Phys A Math Gen 37:R161. https://doi.org/10.1088/0305-4470/37/31/r01
Mitsui T, Crucifix M (2017) Influence of external Forcings on abrupt millennial-scale climate changes: a statistical modelling study. Clim Dyn 48:2729. https://doi.org/10.1007/s00382-016-3235-z
Morr A, Boers N (2024) Detection of approaching critical transitions in natural systems driven by red noise. Phys Rev X 14:021037. https://doi.org/10.1103/PhysRevX.14.021037
Morr A, Riechers K, Rydin Gorjão L, Boers N (2024) Anticipating critical transitions in multidimensional systems driven by time- and state-dependent noise. Phys Rev Res 6:033251
Moyal JE (1949) Stochastic processes and statistical physics. J R Stat Soc Ser B (Methodol) 11:150. https://doi.org/10.1111/j.2517-6161.1949.tb00030.x
Nadaraya EA (1964) On estimating regression. Theory Probab Appl 9:141. https://doi.org/10.1137/1109020
North Greenland Ice Core Projects members (2004) High-resolution record of Northern Hemisphere climate extending into the last interglacial period. Nature 431: 147 https://doi.org/10.1038/nature02805
Pawula RF (1967) Generalizations and extensions of the Fokker-Planck-Kolmogorov equations. IEEE Trans Inf Theory 13:33. https://doi.org/10.1109/TIT.1967.1053955
Pawula RF (1967) Approximation of the linear Boltzmann equation by the Fokker-Planck equation. Phys Rev 162:186. https://doi.org/10.1103/PhysRev.162.186
Planck M (1917) Sitzber. Preuß. Akad. Wiss.. p. 324
Rasmussen SO, Andersen KK, Svensson AM, Steffensen JP, Vinther BM, Clausen HB, Siggaard-Andersen ML, Johnsen SJ, Larsen LB, Dahl-Jensen D, Bigler M, Röthlisberger R, Fischer H, Goto-Azuma K, Hansson ME, Ruth U (2006) A new Greenland ice core chronology for the last glacial termination. J Geophys Res Atmos 111:D06102. https://doi.org/10.1029/2005JD006079

Rasmussen SO, Bigler M, Blockley SP, Blunier T, Buchardt SL, Clausen HB, Cvijanovic I, Dahl-Jensen D, Johnsen SJ, Fischer H, Gkinis V, Guillevic M, Hoek WZ, Lowe JJ, Pedro JB, Popp T, Seierstad IK, Steffensen JP, Svensson AM, Vallelonga P, Vinther BM, Walker MJ, Wheatley JJ, Winstrup M (2014) A stratigraphic framework for abrupt climatic changes during the Last Glacial period based on three synchronized Greenland ice-core records: Refining and extending the INTIMATE event stratigraphy. Quatern Sci Rev 106:14. https://doi.org/10.1016/j.quascirev.2014.09.007

Riechers K, Rydin Gorjão L, Hassanibesheli F, Lind PG, Witthaut D, Boers N (2023) Stable stadial and interstadial states of the last Glacial's climate identified in a combined stable water isotope and dust record from Greenland. Earth Syst Dyn 14:593. https://doi.org/10.5194/esd-14-593-2023

Riechers K, Rydin Gorjão L, Hassanibesheli F, Lind PG, Witthaut D, Boers N (2023) Stable stadial and interstadial states of the last Glacial's climate identified in a combined stable water isotope and dust record from Greenland. Earth Syst Dyn 14:593. https://doi.org/10.5194/esd-14-593-2023

Riechers K, Gottwald G, Boers N (2024) Glacial abrupt climate change as a multiscale phenomenon resulting from monostable excitable dynamics. J Clim 37:2741. https://doi.org/10.1175/JCLI-D-23-0308.1

Risken H, Frank T (1996) The Fokker-Planck equation, 2nd edn. Springer-Verlag, Berlin, Heidelberg. https://doi.org/10.1007/978-3-642-61544-3

Ruth U, Wagenbach D, Bigler M, Steffensen JP, Röthlisberger R, Miller H (2002) High-resolution microparticle profiles at NorthGRIP, Greenland: Case studies of the calcium-dust relationship. Ann Glaciol 35:237. https://doi.org/10.3189/172756402781817347

Ruth U, Wagenbach D, Steffensen JP, Bigler M (2003) Continuous record of microparticle concentration and size distribution in the central Greenland NGRIP ice core during the last glacial period. J Geophys Res Atmos 108:4098. https://doi.org/10.1029/2002JD002376

Ruth U, Bigler M, Röthlisberger R, Siggaard-Andersen ML, Kipfstuhl S, Goto-Azuma K, Hansson ME, Johnsen SJ, Lu H, Steffensen JP (2007) Ice core evidence for a very tight link between North Atlantic and east Asian glacial climate. Geophys Res Lett 34:L03706. https://doi.org/10.1029/2006GL027876

Rydin Gorjão L, Meirinhos F (2019) `kramersmoyal`: Kramers-Moyal coefficients for stochastic, processes. J Open Sour Softw 4:1693. https://doi.org/10.21105/joss.01693

Rydin Gorjão L, Heysel J, Lehnertz K, Tabar MRR (2019) Analysis and data-driven reconstruction of bivariate jump-diffusion processes. Phys Rev E 100:062127. https://doi.org/10.1103/PhysRevE.100.062127

Rydin Gorjão L, Witthaut D, Lind PG (2023) `jumpdiff`: a python library for statistical inference of jump-diffusion processes in observational or experimental data sets. J Stat Softw 105:1. https://doi.org/10.18637/jss.v105.i04

Scheffer M, Bascompte J, Brock WA, Brovkin V, Carpenter SR, Dakos V, Held H, Van Nes EH, Rietkerk M, Sugihara G (2009) Scheffer, Marten and Bascompte, Jordi and Brock, William A. and Brovkin, Victor and Carpenter, Stephen R. Dakos, Vasilis and Held, Hermann and Van Nes, Egbert H. and Rietkerk, Max and Sugihara, George. Nature **461**, 53 https://doi.org/10.1038/nature08227

Schüpbach S, Fischer H, Bigler M, Erhardt T, Gfeller G, Leuenberger D, Mini O, Mulvaney R, Abram NJ, Fleet L, Frey MM, Thomas E, Svensson A, Dahl-Jensen D, Kettner E, Kjaer H, Seierstad I, Steffensen JP, Rasmussen SO, Vallelonga P, Winstrup M, Wegner A, Twarloh B, Wolff K, Schmidt K, Goto-Azuma K, Kuramoto T, Hirabayashi M, Uetake J, Zheng J, Bourgeois J, Fisher D, Zheng D, Xiao C, Legrand M, Spolaor A, Gabrieli J, Barbante C, Kang JH, Hur SD, Hong SB, Hwang HJ, Hong S, Hansson M, Iizuka Y, Oyabu I, Muscheler R, Adolphi F, Maselli O, McConnell J, Wolff EW (2018) Greenland records of aerosol source and atmospheric lifetime changes from the Eemian to the Holocene. Nat Commun 9:1476. https://doi.org/10.1038/s41467-018-03924-3

Seierstad IK, Abbott PM, Bigler M, Blunier T, Bourne AJ, Brook E, Buchardt SL, Buizert C, Clausen HB, Cook E, Dahl-Jensen D, Davies SM, Guillevic M, Johnsen SJ, Pedersen DS, Popp TJ, Rasmussen SO, Severinghaus JP, Svensson A, Vinther BM (2014) Consistently dated records from the Greenland GRIP, GISP2 and NGRIP ice cores for the past 104 ka reveal regional millennial-scale $\delta^{18}O$ gradients with possible Heinrich event imprint. Quat Sci Rev 106:29. https://doi.org/10.1016/j.quascirev.2014.10.032

Silverman BW (1998) Density estimation for statistics and data analysis, 1st edn. Routledge, Boca Raton. https://doi.org/10.1201/9781315140919

Snyder CW (2016) Evolution of global temperature over the past two million years. Nature 538:226. https://doi.org/10.1038/nature19798

Svensson A, Andersen KK, Bigler M, Clausen HB, Dahl-Jensen D, Johnsen SJ, Rasmussen SO, Seierstad I, Steffensen JP, Svensson A, Vinther BM, Davies SM, Muscheler R, Parrenin F, Röthlisberger R (2008) A 60000 year Greenland stratigraphic ice core chronology. Clim Past Discuss 3:1235. https://doi.org/10.5194/cpd-3-1235-2007

Tabar MRR (2019) Analysis and data-based reconstruction of complex nonlinear dynamical systems. Springer International Publishing, Berlin. https://doi.org/10.1007/978-3-030-18472-8

Valdes P (2011) Built for stability. Nature Geosci 4:414. https://doi.org/10.1038/ngeo1200

Van Kampen NG (2007) Stochastic processes in physics and chemistry, 3rd ed., North-Holland Personal Library, Elsevier. https://doi.org/10.1016/B978-0-444-52965-7.X5000-4

Vinther BM, Clausen HB, Johnsen SJ, Rasmussen SO, Andersen KK, Buchardt SL, Dahl-Jensen D, Seierstad IK, Siggaard-Andersen ML, Steffensen JP, Svensson A, Olsen J, Heinemeier J (2006) A synchronized dating of three Greenland ice cores throughout the Holocene. J Geophys Res Atmos 111:D13102. https://doi.org/10.1029/2005JD006921

Virtanen P, Gommers R, Oliphant TE, Haberland M, Reddy T, Cournapeau D, Burovski E, Peterson P, Weckesser W, Bright J, van der Walt S J, Brett M, Wilson J, Millman K J, Mayorov N, Nelson A R J, Jones E, Kern R, Larson E, Carey C J, Polat İ, Feng Y, Moore E W, VanderPlas J, Laxalde D, Perktold J, Cimrman R, Henriksen I, Quintero EA, Harris CR, Archibald A M, Ribeiro A H, Pedregosa F, van Mulbregt P, SciPy 1.0 Contributors, SciPy 1.0: (2020) Fundamental Algorithms for Scientific Computing in Python Nature Methods 17: 261 https://doi.org/10.1038/s41592-019-0686-2

Wang S, Foster A, Lenz EA, Kessler JD, Stroeve JC (2023) Mechanisms and impacts of earth system tipping elements. Rev Geophys 91:e2021RG000757. https://doi.org/10.1029/2021RG000757

Watson GS (1964) Smooth Regression Analysis. Sankhyā Indian J Stati Ser A 26:359

Yang F, Zheng Y, Duan J, Fu L, Wiggins S (2020) The tipping times in an Arctic sea ice system under influence of extreme events. Chaos Interdiscip J Nonlinear Sci 30:063125. https://doi.org/10.1063/5.0006626